New Journal of Physics
The open-access journal for physics

Integrated photonic sensing

N Thomas-Peter[1], N K Langford, A Datta, L Zhang, B J Smith, J B Spring, B J Metcalf, H B Coldenstrodt-Ronge, M Hu, J Nunn and I A Walmsley

Clarendon Laboratory, University of Oxford, Parks Road, Oxford, OX1 3PU, UK
E-mail: n.thomas-peter1@physics.ox.ac.uk

New Journal of Physics **13** (2011) 055024 (20pp)
Received 8 February 2011
Published 31 May 2011
Online at http://www.njp.org/
doi:10.1088/1367-2630/13/5/055024

Abstract. Loss is a critical roadblock to achieving photonic quantum-enhanced technologies. We explore a modular platform for implementing integrated photonics experiments and consider the effects of loss at different stages of these experiments, including state preparation, manipulation and measurement. We frame our discussion mainly in the context of quantum sensing and focus particularly on the use of loss-tolerant Holland–Burnett states for optical phase estimation. In particular, we discuss spontaneous four-wave mixing in standard birefringent fibre as a source of pure, heralded single photons and present methods of optimizing such sources. We also outline a route to programmable circuits that allows the control of photonic interactions even in the presence of fabrication imperfections and describe a ratiometric characterization method for beam splitters, which allows the characterization of complex circuits without the need for full process tomography. Finally, we present a framework for performing state tomography on heralded states using lossy measurement devices. This is motivated by a calculation of the effects of fabrication imperfections on precision measurement using Holland–Burnett states.

[1] Author to whom any correspondence should be addressed.

Contents

1. Introduction

The field of integrated photonics is a promising area for the development of quantum-enhanced technologies with applications being pursued in communications, metrology, simulation and information processing [1–6]. These quantum experiments can be broadly broken up into three stages: state preparation, manipulation and measurement. In recent years, integrated approaches have made substantial advances in each of these three areas, particularly with regard to fibre- and waveguide-based nonclassical light sources [7–21], on-chip quantum circuits [1, 2, 5], [22–27] and integrated detection [28–30].

Perhaps the greatest challenge facing photonic quantum applications is the issue of photon loss, which is generally present in all three of these stages. Loss is particularly critical in quantum information processing (QIP) and quantum-enhanced metrology, where strict thresholds exist for the efficiencies required for a device to out-perform its classical counterpart [31–34]. The most significant contributions to loss in photonic experiments generally arise at the interfaces between different stages of the experiment, e.g. between sources, which may be either spatially or spectrally multimode, and circuits, which often rely critically on low-distinguishability quantum interference. In this example, bulk optics experiments typically require the use of strong, inherently lossy spatial and spectral filtering to achieve the necessary operation fidelities.

The key advantage of integrated optics in overcoming these losses is that it provides the potential for complete spatial and spectral control of the underlying optical field modes. The tight confinement and guided nature of these modes provide exquisite control of their spatial properties, in terms of their transverse profiles as well as paths of propagation. This enables strong interactions between highly indistinguishable optical modes. It is therefore possible to fabricate devices with precise, stable and potentially complex circuit configurations that, because they are small and monolithic, are inherently stable without the need for complex stabilization techniques and provide high-visibility interference [1, 2, 24, 35, 36]. This holds great promise for many photonic QIP applications, which can require complex circuits containing many nested interferometers [37–41], by alleviating the impractical space and stability requirements facing bulk-optics implementations. At the same time, by carefully managing the dispersion properties of integrated devices, either by natural means (material selection) or by engineering design (e.g. poling or mode confinement), it is also possible to exercise fine control over the spectral properties of the optical modes. Such control can be

used, for example, to design spectrally pure, heralded single-photon sources [9, 20, 21, 42, 43], a critical requirement of scaleable photonic QIP systems.

The holy grail of integrated photonics is a single device containing an entire photonic quantum experiment, state preparation, manipulation and measurement. Such an approach, however, faces an enormous challenge: a fully integrated platform requires the marriage of many fundamentally different, often incompatible technologies within a single material substrate. For example, thermo-optic phase control [1, 2, 44] would clearly be impossible on a device that is being cooled to cryogenic temperatures (mK) in order to operate a superconducting transition-edge sensor (TES), which currently provides the leading performance in terms of both quantum efficiency and photon-number resolution.

An alternative approach, achievable within the current state of the art, is to employ a more modular solution, where each stage of the experiment is performed using the technology platform that is most suited to the task. The main task of integration is then simply to ensure that the interface between platforms does not introduce an unacceptable level of loss. This is not an unreasonable target, however, since the unprecedented spatial-mode control available in integrated architectures already provides the means of optimizing the coupling efficiencies between platforms. Such an approach also presents a strong advantage in terms of flexibility. This cluster of technologies would become a platform on which large-scale complex experiments could be performed, enabling progress both in practical applications of quantum enhanced technologies and in fundamental research, and could include components for active phase control [1, 2], Bragg reflectors for frequency filtering, and the building of cavities [42] and on-chip micro-fluidic capillaries for interfacing photonic systems with fluids or fluid suspensions [45], to name just a few examples.

In this paper, we will focus on the specific example of sensing in a real-world integrated photonic device via (linear) quantum interferometry, as it provides a clear example of the stringent requirements placed upon the different modules. We will follow the chain of state generation, manipulation and detection, discussing in turn the key requirements for and issues surrounding each. We will also introduce a technique for characterizing optical elements in an integrated photonic device, as well as a framework that allows tomographic reconstruction of a heralded state, including all photon-number subspaces.

2. Quantum sensing—an example context

Quantum-enhanced metrology is concerned with a single task: preparing a quantum state that is sensitive to a parameter, ϕ, and implementing a measurement on that state so that the uncertainty in the measurement of the parameter, $\Delta\phi$, is lower than the uncertainty that would be obtained using the same number of classical resources. Typically, only the scaling behaviour of $\Delta\phi$ with the number of particles in the state, N, is considered, since at large enough N a class of states that provides only a constant factor improvement can always be beaten by one that has a more favourable scaling. The tightest known limit on precision is given by the Heisenberg limit (HL), $\Delta\phi \geqslant \Delta\phi_{\mathrm{HL}} = 1/\sqrt{\nu}N$, where ν is the number of experimental trials.

The situation we will consider in this paper is shown schematically in figure 1(a). For any given state and measurement, the input state ρ evolves to become $\rho(\phi)$ and a measurement is performed with outcomes represented by the operators $\{\hat{\Pi}_\gamma\}$. Performing ν trials provides a data set and the precision with which ϕ can be estimated from this data set, $\Delta\phi$, is bounded by the Cramér–Rao bound (CRB), $\Delta\phi \geqslant \Delta\phi_{\mathrm{CRB}} = 1/\sqrt{\nu F(\phi)}$. Here, $F(\phi)$ is the Fisher information

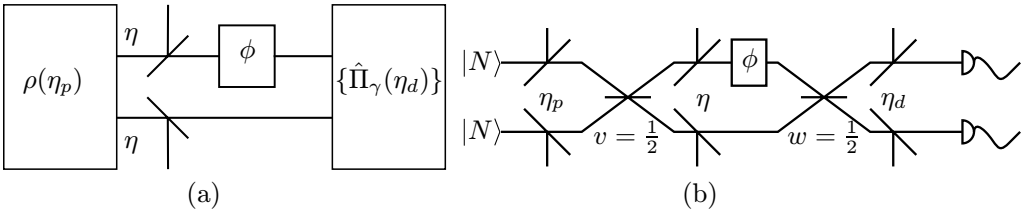

Figure 1. Schematic representation of a typical metrology scenario. (a) General two-mode interferometer with inefficient state preparation, two lossy modes and inefficient detection. (b) A detailed equivalent network involving a Mach–Zehnder interferometer, with the losses specified by individual beam splitters of transmissivity η_p, η and η_d.

(FI), a measure of the information that can be obtained about ϕ from the data set. The CRB can be saturated at large ν by maximum likelihood estimation. Interestingly, a measurement-independent version of the FI can be found by maximizing over all physical measurements giving the quantum Fisher information (QFI), $F_Q(\phi)$. This, in turn, leads to the lowest possible bound on the precision obtainable using a given state, the quantum Cramér–Rao bound (QCRB), $\Delta\phi \geqslant \Delta\phi_\mathrm{QCRB} = 1/\sqrt{\nu F_Q(\phi)}$ [46].

To judge whether or not a device could perform better than its classical counterpart, we must compare the QCRB of the prepared state to that of N completely uncorrelated photons. In the ideal situation of a perfectly transmissive device, this leads to the standard quantum limit $\Delta\phi \geqslant \Delta\phi_\mathrm{SQL} = 1/\sqrt{\nu N}$. In the presence of loss, however, this becomes the standard interferometric limit (SIL) [47], $\Delta\phi \geqslant \Delta\phi_\mathrm{SIL} = 1/\sqrt{\nu\eta\eta_\mathrm{d}N}$, where η and η_d model the transmission inside the interferometer and detection efficiency, respectively (see figure 1). The SIL is unaffected by the parameter η_p due to the fact that a state which saturates the SIL, the phase-averaged coherent state, only undergoes a scaling in average photon number with loss. It is therefore considered that a phase-averaged coherent state with arbitrary average photon number can be prepared perfectly. In general, however, all losses including η_p play a crucial role in the QCRB for any given prepared state. If $\Delta\phi_\mathrm{QCRB} \leqslant \Delta\phi_\mathrm{SIL}$, then the state that is prepared could perform better than its classical counterpart, but it will only do so if an appropriate measurement scheme is implemented. If such a scheme is implemented, $\Delta\phi_\mathrm{CRB} \leqslant \Delta\phi_\mathrm{SIL}$ and the device truly does outperform its classical counterpart.

3. State generation

The most widely studied state in quantum-enhanced metrology is the N00N state [1, 2], [48–52]. This path-entangled state is a superposition of $N(0)$ photons in one mode with $0(N)$ photons in the other and, under perfect transmission, it saturates the HL. It does, however, suffer from a major drawback in the lossy case. When even a single photon is lost from the N00N state, the remaining state is entirely insensitive to the phase ϕ. Thus all photons must make it through the device and be detected in order for information to be gained about ϕ, an exponentially unlikely event for increasing N [33]. Schemes for generating high-N N00N states are also complex, often requiring many nonlinear elements [53] or carefully aligned cavities [54]. Optimally loss-tolerant N-photon states have also been studied [47, 55], but preparation strategies and detection schemes for these states have not yet been found and knowledge of the exact channel loss would also be required.

In contrast to N00N states and optimal states, the Holland–Burnett (HB) or twin–Fock states [56] provide a much simpler route to quantum-enhanced metrology, while retaining near-optimal loss tolerance. An HB(N) state is prepared by interfering two N-photon Fock states at a 50 : 50 beam splitter (see figure 1(b)). The resulting state retains phase sensitivity under loss both before and after this beam splitter and hence does not need perfect transmission to be useful. As well as this, the QFI for the HB(N) state is attained through the use of photon-number-resolving detectors, regardless of the loss parameters [34]. The requisite Fock states can be prepared by heralding N photons from two 2-mode photon-number-correlated sources, for example based on spontaneous parametric downconversion (SPDC) or spontaneous four-wave mixing (SFWM). A recent work [34] has put bounds on the η_{p}, η and η_{d} that are necessary for beating the classical limit, showing that for $\eta_{\mathrm{d}} = 0.6$ and $\eta = 0.95$, a state preparation efficiency of $\eta_{\mathrm{p}} \geqslant 0.91$ is required. Even for the best currently available detectors with $\eta_{\mathrm{d}} = 0.98$, the requirement on η_{p} is relaxed only to $\eta_{\mathrm{p}} \geqslant 0.71$. This puts extremely challenging bounds on the current state of the art for quantum sources.

The key ingredient for generating HB(N) states is the creation of N-photon Fock states with sufficient purity to achieve the quality of quantum interference required for high-fidelity state production. More generally, if these sources are to be useful in a scaleable way for integrated photonics quantum technologies, they will need to be either on-demand or heralded. A heralded source can be converted into an on-demand source using a controllable quantum memory with a high time–bandwidth product [57–59]. The important characteristics of such sources are heralding or preparation efficiency, purity and indistinguishability of the photons produced (in polarization, spatial and temporal degrees of freedom). In addition, in order to avoid excess loss at the interface with the quantum circuit, the photon mode structure should be compatible with integrated devices, particularly in terms of spatial overlap, for ensuring optimal performance. If the photons produced by these sources do not adhere to strict requirements for these parameters, the performance of the quantum protocols rapidly decays (see e.g. [60, 61]).

One of the most common and most successful ways of producing heralded photonic quantum states makes use of nonlinear processes such as SPDC or SFWM. These are robust, room-temperature processes that can produce large numbers of photons for moderate pump powers. Because of the strong photon-number correlations induced by the nonlinear interaction, they can be used to produce high-quality heralded Fock states. Unfortunately, however, the generated state also contains terms with more than the desired number of photon pairs in a single pulse. This ambiguity leads to dramatically reduced performance in many QIP applications if standard avalanche photodiodes (APDs) are used as heralding detectors, because they are unable to distinguish between different photon-number terms [61]. In the ideal case, this problem can be largely mitigated by using photon-number-resolving heralding detectors [29, 62] instead. In the presence of loss, however, it becomes exacerbated and cannot simply be overcome by using a stronger pump to increase the count rate. Loss acts to weaken the photon-number correlations in the generated state and therefore decrease the quality of interference exhibited by the heralded Fock states. Furthermore, although increasing the pump does increase the signal strength, it can increase the strength of the noise-contributing higher-order terms by a larger proportion, because although they occur less frequently than the signal term, they are often more likely to be detected when they do occur. Thus, quantum state production must be optimized to provide the highest possible heralding efficiency.

In general, photon pair sources based on SPDC or SFWM produce pairs that display spectral entanglement, and this manifests itself in a joint spectral amplitude (JSA) which is

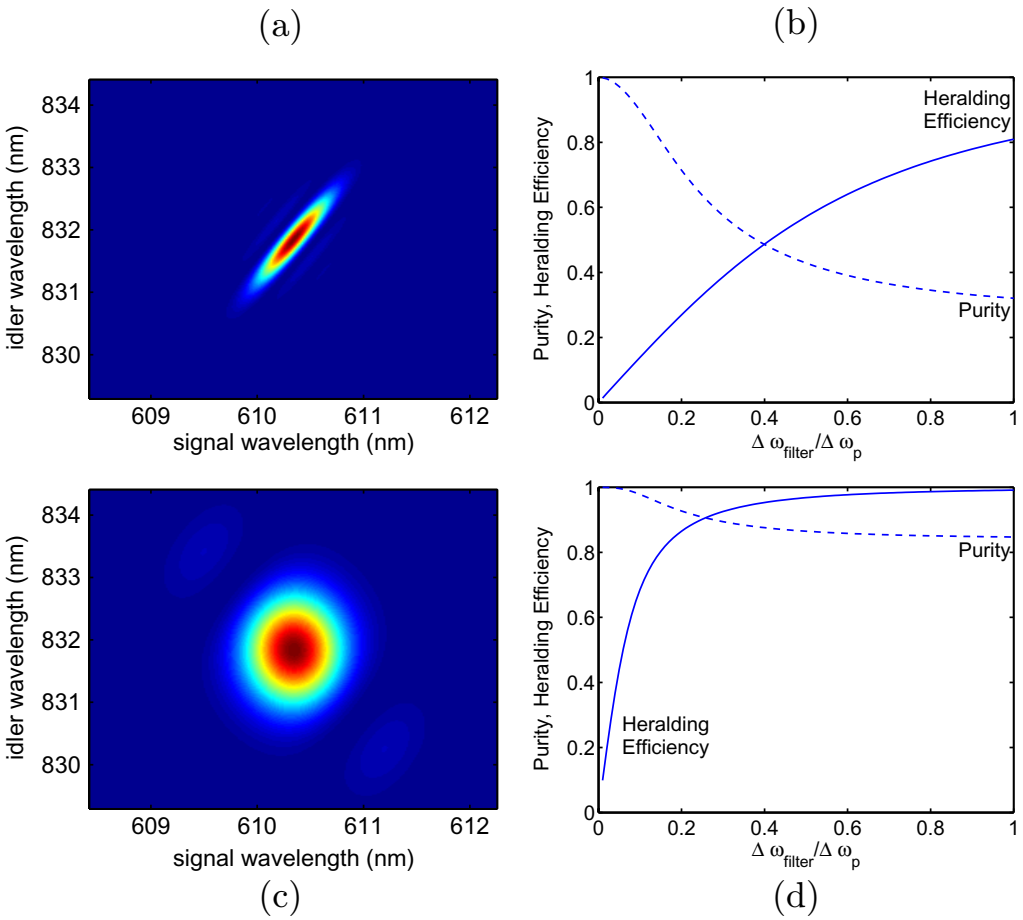

Figure 2. (a) A typically correlated joint spectrum for an SFWM photon-pair source. (b) Heralding efficiency (solid) and purity (dashed) as a function of the Gaussian filter bandwidth (in units of the pump bandwidth) for the correlated case. (c) Joint spectrum for an SFWM photon-pair source with matched phase matching and pump bandwidths. (d) Heralding efficiency (solid) and purity (dashed) as a function of the Gaussian filter bandwidth (in units of the pump bandwidth) for the matched bandwidths case.

not factorable. A typical example of such a JSA is shown in figure 2(a), where the correlations are clearly visible as correlations in the frequencies of the two photons. Consequently, although detecting N photons in one mode heralds the presence of N photons in the other, the heralding detectors are typically spectrally nonselective and therefore project these heralded photons into a spectrally mixed state. The usual technique for removing these spectral correlations is to use narrow spectral filters, but this improvement in purity comes at the expense of decreased heralding efficiency, i.e. decreased η_p, which therefore also increases the effects of noise in the experiment.

The trade-off between heralding efficiency and spectral purity for the highly correlated joint spectral amplitude of figure 2(a) is shown in figure 2(b). The purity of the unfiltered heralded signal photon is 27%. Using spectral filters that only pass a symmetric portion of the joint spectrum dramatically decreases the heralding efficiency of the source so that, for a purity of 95%, the heralding efficiency is limited to 9.7%.

A promising route to generating heralded pure-state single photons with high efficiency and purity is to directly engineer the nonlinear optical interaction [13], [63–68]. In these approaches, an intense pump is converted into a pair of photons, denoted as signal (s) and idler (i) mediated by the nonlinear medium. This process must obey both energy and momentum conservation, which generally leads to spectral and momentum correlations. However, by carefully choosing material parameters and pump configurations, these correlations can be eliminated. SFWM utilizing birefringent phase matching in optical waveguides offers several advantages over other nonlinear optical sources, such as perfect spatial mode matching with existing photonic circuitry allowing low-loss integration, flexible tuning of the signal and idler central wavelengths through birefringence, and tolerance to waveguide properties [18, 69]. In this scenario, the pump propagates along the fast axis while the signal and idler photons are produced along the orthogonal slow axis of the waveguide. The wave-vector mismatch includes a term proportional to the birefringence and pump central frequency. Thus, by adjusting the pump central frequency and birefringence one can tune the central frequencies of the signal and idler photons. To achieve the nearly factorable states required for heralding pure-state single photons with birefringent phase matching, the pump bandwidth must be balanced with the phase matching bandwidth, which is determined by the interaction length [18, 69]. A typical JSA produced under such balanced conditions is shown in figure 2(c). The correlations are significantly reduced despite the remaining lobes that result from the sinc-like form of the phase-matching function. Figure 2(d) shows the effect on the heralding efficiency and purity of applying spectral filters to this JSA. For a purity of 95%, heralding efficiency in this case is greater than 80%, directly demonstrating the higher intrinsic purity of the source.

4. Manipulation

Once pure single photons have been created, they must be manipulated in such a way as to implement, for example, logic gates or a metrology scheme. Only two components are necessary in order to implement all unitary operations: beam splitters and phase shifters. Beam splitters can be constructed using evanescent [5, 24], x-couplers [1] or multimode interference devices [26], while phase shifters can be implemented by thermo-optic [1, 2] or electro-optic [70] means.

Evanescent couplers are fabricated by bringing together two waveguides so that the evanescent fields of the two modes overlap, creating a coupling between them. The field then flips back and forth between the modes as they propagate in parallel. The rate of this flipping is determined by the overlap of the two modes, which is dependent on the separation of the waveguides. For such a device with a given waveguide separation, the splitting ratio is determined by the length of the coupling region and the wavelength being used. They can be produced using either lithographic or direct-write techniques. X-couplers are produced by physically crossing the waveguides at a shallow angles giving a splitting ratio that is a function of this angle. Direct write techniques must be used to fabricate x-couplers since to produce this shallow angle, sharp features in the guiding structure are required, which cannot currently be produced using lithographic techniques.

A detailed comparison of thermo-optic phase shifters against electro-optic versions is yet to be performed for quantum devices, because although electro-optic phase shifters are common in commercially available classical integrated devices, they have not been

demonstrated in an integrated photonic device. They have several potential advantages over their thermo-optic counterparts; most notably a reduced switching time that, if combined with integrated quantum memories, could provide a route to one-way photonic QIP.

For the specific example considered in this paper, it is critical to be able to produce beam splitters with accurate splitting ratios. The splitting ratios of the two beam splitters shown in figure 1(b) affect both the fidelity of the HB state produced and the measurement scheme that is implemented, limiting the FI that can be obtained.

In order to show this, we begin by defining the angular momentum operators in the Schwinger representation as

$$J_x = \tfrac{1}{2}(\hat{a}^\dagger b + a\hat{b}^\dagger),\ J_y = \tfrac{1}{2i}(\hat{a}^\dagger b - a\hat{b}^\dagger),\ J_z = \tfrac{1}{2}(\hat{a}^\dagger a - \hat{b}^\dagger b), \tag{1}$$

$$J^2 = J_x^2 + J_y^2 + J_z^2. \tag{2}$$

In a basis defined by the mutual eigenbasis of J^2 and J_z, the ideal input state $|N\rangle_a|N\rangle_b$ appears as $|N, 0\rangle$. In this picture, the phase operator is [71]

$$P(\phi) = \mathrm{e}^{\mathrm{i}\phi J_z}, \tag{3}$$

while a beam splitter is given by

$$B(\theta) = \mathrm{e}^{-2\mathrm{i}\theta J_x}, \tag{4}$$

where $\sin^2\theta = v$ is the input beam splitter transmissivity. The effective phase operator is then given by

$$\tilde{P}(\phi) = B(\theta)P(\phi)B(\theta)^\dagger = \mathrm{e}^{\mathrm{i}\phi(\cos 2\theta J_z - \sin 2\theta J_y)}, \tag{5}$$

where we have used the SU(2) commutation relations of the angular momentum operators. For a 50/50 beam splitter $\theta = \pi/4$, in which case the effective role of the beam splitter and the phase combined is to effect a rotation about the $-J_y$ axis. In general, this axis of rotation is given by (5), and given that the input state points along the z-axis, the radius of rotation shrinks by a factor of $\sin 2\theta = 2\sqrt{v(1-v)} \leqslant 1$, as depicted in figure 3(a). The net effect is to suppress the phase picked up by the state $|N\rangle_a|N\rangle_b$ with the beam splitter ratio v. Since the phase picked up is suppressed by this factor, the precision is also suppressed by the same amount so that the QFI in this case is given by

$$F_{\mathrm{Q}} = 4N(N+1)v(1-v). \tag{6}$$

This shows that the best attainable precision is provided by a $50:50$ input beam splitter. In that case, we know that this can be attained with another $50:50$ beam splitter at the other end of the interferometer and an $|N\rangle\langle N| \otimes |N\rangle\langle N|$ detection (in the loss-less case). For every other situation, however, there remains the issue of attaining the reduced bound provided by (6). Allowing for a general beam splitter at the detection end makes the calculation somewhat involved, so we restrict ourselves to the $|1\rangle_a|1\rangle_b$ case. Then the classical FI, F, as a function of the input beam splitter v and output beam splitter w is shown in figure 3(b), assuming that we have perfect photon-number-resolving detectors.

In practice, fabrication tolerances result in beam splitters that do not have the reflectivity they were designed for. Fortunately, the Mach–Zehnder interferometer (MZI) provides a solution, since the combination of two beam splitters and a phase shifter can be thought of

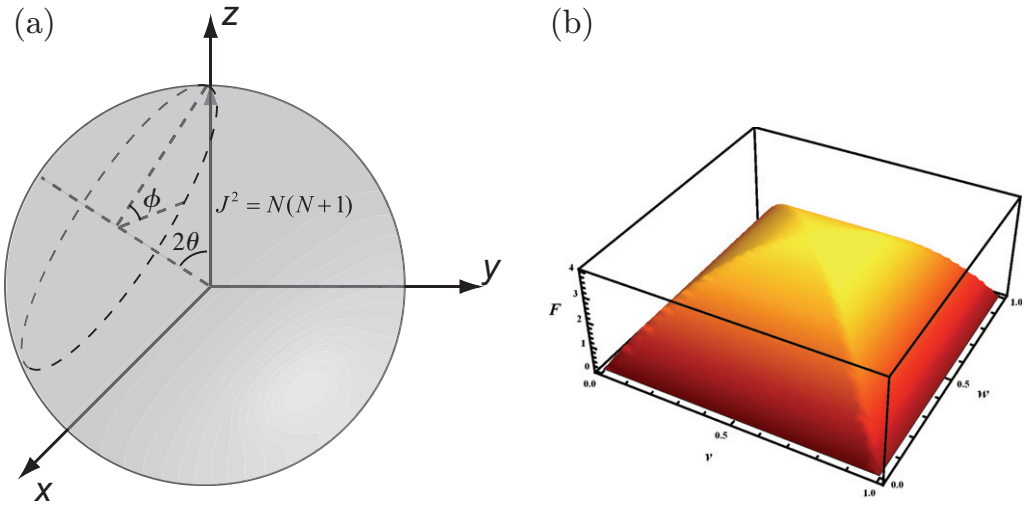

Figure 3. (a) The effect of varying v and w on the effective phase operator. (b) The Fisher information of the state generated by $|1\rangle_a|1\rangle_b$ impinging on a beam splitter of reflectivity v when a detection event $|1\rangle\langle 1| \otimes |1\rangle\langle 1|$ occurs after a beam splitter of reflectivity w, maximized over the phase ϕ.

as a single beam splitter whose reflectivity, v_{eff}, is a function of the applied phase,

$$v_{\text{eff}} = vw + (1-v)(1-w) + 2\sqrt{v(1-v)w(1-w)}\cos\phi. \tag{7}$$

If both beam splitters were to have a splitting ratio of $1/2$, then by adjusting the phase, the full range of reflectivities from perfectly reflective to perfectly transmissive can be realized. As the reflectivities of the beam splitters vary away from $1/2$, the effective reflectivities that can be reached by tuning the phase is reduced; however, this technique dramatically increases the robustness of the system to fabrication tolerances. Figure 4 shows the values of the two beam splitters for which reflectivities of $1/2$ and $1/3$ can be obtained. In principle, one could even combine four nominally $50:50$ beam splitters with three phase shifters to produce a single programmable beam splitter that is tunable over the full range $0 \leqslant v_{\text{eff}} \leqslant 1$.

Since a variation in beam splitter reflectivities is inevitable, a way of accurately characterizing them is necessary in order to calibrate and predict the behaviour of any device. Full process tomography becomes extremely complex and unwieldy for large systems so it is necessary to characterize components individually to build up the characteristics of the device. Here we present a ratiometric characterization technique that allows the measurement of the splitting ratio independently of the input and output coupling efficiencies associated with launching light into and collecting light from the device. The situation being considered here is shown schematically in figure 5. Although only a single beam splitter is shown, this technique can be applied to any beam splitter embedded in a larger circuit as long as both inputs to and both outputs from the beam splitter can be accessed independently.

Initially, coherent light with intensity I is coupled into mode a. This light propagates through the circuit and is detected at the outputs, having experienced propagation, coupling and detection losses. These can be represented by a single transmissivity at the inputs, η_a and η_b, and a single transmissivity at the outputs, η_c and η_d. At the outputs, two intensities are measured, I_{ac} and I_{ad} in modes c and d, respectively. These intensities can be written as a function of the

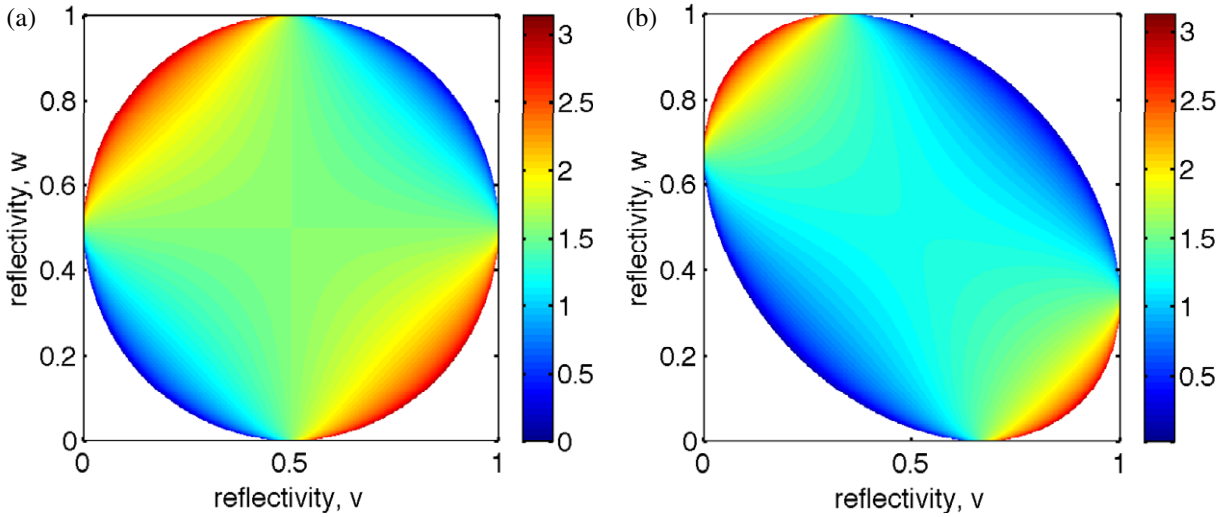

Figure 4. (a) The values of v and w for which an effective reflectivity of $1/2$ can be reached. (b) The values of v and w for which an effective reflectivity of $1/3$ can be reached. In both plots the reflectivity combinations in the white areas do not allow tuning to the target effective reflectivity. The phase required to reach the target effective reflectivity is represented by colour.

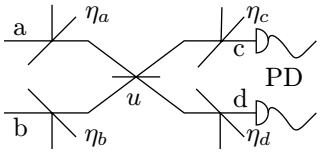

Figure 5. Schematic representation of a device consisting of a single beam splitter of reflectivity u, with input and output coupling efficiencies modelled by beam splitters with η_a, η_b for input coupling transmissivity, and η_c, η_d for output coupling transmissivity. The spatial modes are labelled a, b, c and d. Detection is performed by photodiodes (PD).

transmissivities, beam-splitter reflectivity and the initial intensity,

$$I_{ac} = \eta_a u \eta_c I, \tag{8}$$

$$I_{ad} = \eta_a (1-u) \eta_d I. \tag{9}$$

Similarly, the same light is coupled into mode b, giving

$$I_{bc} = \eta_b (1-u) \eta_c I, \tag{10}$$

$$I_{bd} = \eta_b u \eta_d I. \tag{11}$$

Finally, by taking the ratio $r = I_{ad} I_{bc} / I_{ac} I_{bd}$ and solving for u, taking the solution, that gives $0 \leqslant u \leqslant 1$, we obtain

$$u = \frac{1}{1+\sqrt{r}}. \tag{12}$$

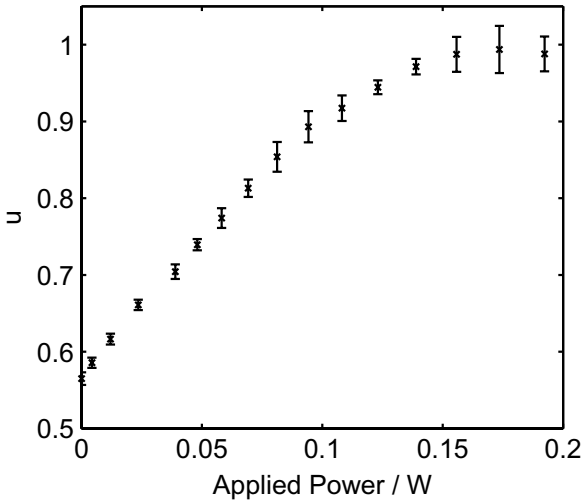

Figure 6. The effective reflectivity of an MZI as a function of the power dissipated by a thermo-electric phase shifter. Characterization was performed using a ratiometric technique, which is independent of coupling losses (see text).

Figure 6 shows the results of this technique being applied to an MZI that is acting as a single, programmable beam splitter. The maximum beam splitter reflectivity reached is 0.993. The range of applied powers is limited in this case due to the robustness of the particular device used. Fitting equation (7) to a full fringe would allow the individual beam splitter reflectivities to be obtained; however, this equation is symmetric under exchange of the two reflectivities and so although the values can be obtained, the ordering is ambiguous. In order to resolve this ambiguity, we must be able to measure one of the beam splitter ratios directly. As well as this, the individual inputs and outputs of some beam splitters in QIP circuits are not independently accessible, for example in a controlled-NOT gate where only three beam splitters may be characterized in this way [36].

This problem is alleviated by using a camera to collect light scattered out of the mode in the transverse direction. The outputs of a particular beam splitter can then always be independently accessed, drastically increasing the applicability of the above technique. In this situation, the light observed at the camera is a proportion of the light propagating in the mode. As with the ratiometric technique outlined above for output intensities measured with a linear detector, the proportion scattered does not need to be constant for different paths since the ratiometric analysis gives a reflectivity that is independent of the scattering ratio and coupling efficiency. Consequently, however, the camera used must display a linear response and the image of the output modes must not change position on the camera sensor so that the pixel efficiency is constant when coupling into each input.

5. Measurement and detection

The final stage in any photonic experiment is detection. High-quality, quantum-limited measurements are an essential requirement for demonstrating explicitly nonclassical behaviour in a quantum experiment, and this is characterized by the detectors, the measurement apparatus as a whole and by the way that apparatus is utilized in the experiment. Quantum-limited

detection in photonics experiments is normally carried out using photon counting. As discussed above in relation to state preparation, in the metrology example the detection must be very efficient if the quantum device is to outperform its classical counterpart in terms of overall precision [33, 34]. Indeed, even with detector efficiencies close to 100%, the constraints placed on preparation efficiencies and propagation losses for achieving true quantum-enhanced operation are extremely stringent and have not been demonstrated by any existing experiment.

The standard workhorse of photon-counting experiments is the APD, a binary ('zero/many') detector that is readily commercially available. Unfortunately, typical quantum efficiencies for silicon APDs reach at maximum up to 60% for wavelengths around 800 nm, where they have a peak in sensitivity. By contrast, efficiencies of up to 98% [72] can be reached with the recently developed superconducting TES detectors, with the additional advantage that they also provide direct photon-number resolution. Both APDs and TES detectors are generally operated in a fibre-coupled configuration, making them well suited to a modular integrated-photonics platform. A major drawback with the still-emerging TES technology is that the detectors currently have to operate at ultracold cryogenic temperatures (typically mK). While the efficiency is still limited, another way to achieve many of the benefits of photon-number resolution is via time multiplexing [29, 62]. Time-multiplexed detectors (TMDs) are pseudo-photon-number-resolving detectors that utilize standard, commercial components and can be operated straightforwardly at room temperature. They work by dividing the input signal into a number of distinguishable temporal modes, which are then monitored by standard APDs. The scaleability of this technique is largely limited by the dead-time of the APDs, which is typically around 50 ns for current APDs. This currently leads to large readout-response times and therefore limits the repetition rate at which they are able to operate. TMDs only provide pseudo-photon-number resolution, because there is still a probability that more than one photon will arrive at an APD in a single temporal mode—they only provide unambiguous photon-number resolution in the limit of many more temporal modes than incoming photons. These effects can in many cases be mitigated, however, by appropriately characterizing the behaviour of the detectors in advance via detector tomography [73–75].

Detector tomography is a general technique that uses weak-coherent input states to probe the detector operation and reconstruct the individual measurement operators representing each possible detector outcome, including their description in the photon-number basis. To date, this technique has been used to characterize the behaviour of both a standard APD and a TMD [73, 74]. An important aspect of detector tomography is that it provides a direct estimate of detection efficiency [75], which, as we have already discussed, is key to understanding and interpreting observations of quantum effects in experiments (e.g. metrology), particularly in the presence of loss.

A common task that is often necessary in the building and characterization of photonic circuits for quantum applications is quantum state tomography [76–78]. In order to understand the performance of the quantum device, it is important to be able to estimate the form of the input quantum state on which that performance depends. This is equally true for integrated photonics applications. Traditionally, photonic experiments rely on post-selection, where the state is assumed to be within a specific photon-number subspace. This means that loss in the measurement device used to perform state tomography can, for the most part, be ignored. Unfortunately, however, this is not sufficient in many situations, such as the metrology example that we have considered here. In this case, phase information can generally be acquired to some

degree from all photon-number subspaces, particularly in the case of 'classical' coherent input states, against which any quantum device must be measured to determine whether it improves upon the classical limit. The ability to acquire some level of phase information from lower photon-number terms is a signature of loss-tolerant probe states, such as the optimally loss-tolerant state [47, 55] and the HB states [56]. Unusually, this is not the case with the N00N state, which is an indication of its fragility to loss. However, because of the effects of loss, even in this case it is critical to characterize the complete input state, including the contributions from all photon-number subspaces, in order to obtain a genuine estimate of the performance of the quantum device. Once the complete density matrix of the input state is known, this can be used to calculate the QCRB, which defines the usefulness of the prepared state for phase estimation. In order to reconstruct the complete density matrix of a quantum state, two key experimental ingredients are required: firstly, a heralded source of input states to probe the contribution from the vacuum subspace, and secondly, a measurement apparatus, which provides some level of photon-number resolution, so that different Fock subspaces can be interrogated.

In general, a state tomography experiment can be described by a set of N_α detection apparatus settings, labelled here with α, each of which has associated with it a set of N_γ outcomes, labelled here with γ so that $N_\alpha N_\gamma$ measurements are implemented. In photonic experiments, the outcomes are usually a particular combination of physical detectors firing simultaneously ('in coincidence'). The measurements implemented are modelled by a set of positive operator value measure (POVM) elements $\{\hat{\Pi}_\gamma\}_\alpha$. In this scheme, the outcomes for each setting are complete so that for every α, $\sum_\gamma \hat{\Pi}_\gamma = \mathbb{1}$. The settings must be chosen so that the POVM elements span the space of states, allowing reconstruction of any state in the space. In general there are optimal ways to choose both the settings and the amount of time spent measuring at each setting, which is sometimes referred to as optimal experiment design [79–82].

Once the settings have been chosen, the measurements are carried out, usually with a fixed time spent at each α. In this time, the number of events corresponding to each outcome γ are recorded, giving a set of counts $\{n_\gamma\}_\alpha$. The probability that any state, represented in density matrix form as ρ, could produce the observed counts is then given by the likelihood function,

$$\mathcal{L} = p(\{n_{\alpha\gamma}\}|\rho), \tag{13}$$

where $\{n_{\alpha\gamma}\}$ denotes the set of all measured counts at all settings. We discuss here the most common state reconstruction technique, known as maximum likelihood estimation, where the estimated ρ is determined by maximizing the value of the likelihood function [77, 78].

The exact form of $\mathcal{L}$ is dependent on the system generating the state. With heralded state generation, the number of times that the state has been prepared for each setting, n_α, is known so that for each herald signal a result is collected. The number of heralds limits the values of n_γ so that $\mathcal{L}$ is most appropriately described by a multinomial distribution,

$$\mathcal{L} = \prod_{\alpha\gamma} C_\alpha(\{n_\gamma\}_\alpha) p_{\alpha\gamma}^{n_{\alpha\gamma}}, \tag{14}$$

where C_α is a multinomial factor that accounts for the number of ways the observed n_γ could have occurred for each setting and $p_{\alpha\gamma} = \mathrm{tr}(\rho\hat{\Pi}_{\alpha\gamma})$. Since n_α is known for each setting, only $N_\gamma - 1$ measured counts, or their corresponding probabilities, are independent variables in the maximum likelihood optimization. This can be expressed as the constraint equation $\sum_\gamma n_{\alpha\gamma} = n_\alpha$. This maximization can be performed directly using an iterative technique [78].

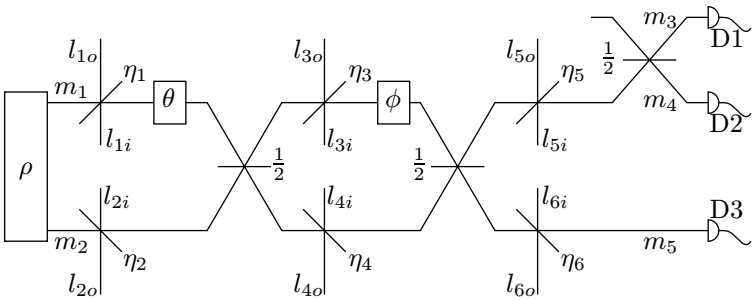

Figure 7. A typical setup used to perform state tomography on ρ. ρ is assumed to be a single polarization photonic state in two spatial modes. An MZI and two phase shifters allow a tomograpically complete set of measurements to be made. Detection is performed by APDs (D1–D3). The spatial modes that lead to detectors are labelled m_1–m_5, while loss modes are labelled $l_{1\mathrm{i}}$–$l_{6\mathrm{i}}$ and $l_{1\mathrm{o}}$–$l_{6\mathrm{o}}$.

If n_α is large and $p_{\alpha\gamma}$ is small, the multinomial form can be approximated by a product of $N_\alpha(N_\gamma - 1)$ Gaussian distributed variables,

$$\mathcal{L} = \prod_{\alpha\gamma} \frac{1}{\sqrt{2\pi\sigma_{\alpha\gamma}^2}} \exp\left\{ -\frac{(n_{\alpha\gamma} - n_\alpha p_{\alpha\gamma})^2}{2\sigma_{\alpha\gamma}^2} \right\}, \tag{15}$$

where $\sigma_{\alpha\gamma} = n_\alpha p_{\alpha\gamma}(1 - p_{\alpha\gamma}) \approx n_\alpha p_{\alpha\gamma}$ for small $p_{\alpha\gamma}$. Typical current devices exhibit high loss, so that the vacuum component of any heralded state will contain a large population. While this might be expected to take us out of the regime of small $p_{\alpha\gamma}$, we are still free to choose which outcome probability is the 'dependent variable' for each measurement setting. Using the corresponding constraint equation, we therefore choose to eliminate the vacuum term, leaving only the lower probability terms that still satisfy the small p approximation. Expressing the likelihood function in this form ultimately allows one to express the problem in a weighted least-squares form, which can be converted into a semi-definite programme so that the well-developed tools of convex optimization can be employed [83].

A necessary part of this optimization is knowledge of the POVM elements that model the particular outcomes observed. Since we wish to be able to reconstruct all photon number subspaces, we need measurements that access all photon-number subspaces. In the case of a perfectly efficient, perfectly photon-number-resolving device, it can be precisely known which photon-number subspace is being projected onto. In the presence of any loss, however, even photon-number-resolving detectors project onto multiple photon-number subspaces because registering a single photon could be due to, for example, two photons where one is lost. The exact value of the loss in the measurement device specifies the mixture of photon-number subspaces being projected onto, and hence must be known if a state is to be accurately reconstructed. As an example, we will consider the device shown in figure 7, which provides tomographic measurements suitable for characterizing the HB(1) state. The detectors used are perfect APDs, which have a POVM set of $\{|0\rangle\langle 0|, \mathbb{1} - |0\rangle\langle 0|\}$, meaning that either they do not fire and therefore project onto the vacuum, or they fire, in which case at least one photon is present but it is not known how many. This device is insensitive to coherences between components in different photon-number subspaces. Fortunately, however, these coherences cannot affect the measurement statistics in our system, or indeed in any system comprised of imperfect state

preparation, lossy linear optical interactions and inefficient detection. This is true because all linear optical components conserve photon number by definition (i.e. they operate only within each photon number subspace), loss is always incoherent, and photon-counting detectors project onto incoherent mixtures of components from within these different subspaces. A state reconstructed in this way therefore provides sufficient information to predict all measurement outcomes of any subsequent system acting on that state using linear optical interactions and photon-counting measurement.

For the system in figure 7, there are five possible outcomes: no clicks; a click at either detector 1 (D1) or detector 2 (D2); a click at detector 3 (D3); a click at D1 and D2; a click at D1 and D3, or D2 and D3. These are labelled $\hat{\Pi}_{\gamma}^{(\mathrm{out})}$ where $\gamma = 1$–5. Losses in the system are modelled by beam splitters with reflectivities η_1 to η_6. Detector inefficiencies are incorporated into the losses directly before the detectors (η_5 and η_6) [84]. The modes leading to detectors are labelled with m_1 to m_5, while the loss modes are labelled $l_{1\mathrm{o}}$ to $l_{6\mathrm{o}}$ for the 'outer' modes and l_{1i} to l_{6i} for the 'inner' modes. Typically, the projectors for the detectors are back-propagated and expressed in terms of projectors at the input of the measurement device, and the η_i are set to 1. If losses are considered, however, one must back propagate both the click projectors for the APDs and identity projectors for each of the outer loss modes because they are not monitored. The output POVM set is given by the projectors

$$\hat{\Pi}_1^{(\mathrm{out})} = \mathbb{1}_{l_{1o}} \otimes \ldots \otimes \mathbb{1}_{l_{6o}} \otimes |0\rangle\langle 0|_{m3} \otimes |0\rangle\langle 0|_{m4} \otimes |0\rangle\langle 0|_{m5}, \tag{16}$$

$$\hat{\Pi}_2^{(\mathrm{out})} = \mathbb{1}_{l_{1o}} \otimes \ldots \otimes \mathbb{1}_{l_{6o}} \otimes [(\mathbb{1} - |0\rangle\langle 0|_{m3}) \otimes |0\rangle\langle 0|_{m4} + |0\rangle\langle 0|_{m3} \otimes (\mathbb{1} - |0\rangle\langle 0|_{m4})] \otimes |0\rangle\langle 0|_{m5}, \tag{17}$$

$$\hat{\Pi}_3^{(\mathrm{out})} = \mathbb{1}_{l_{1o}} \otimes \ldots \otimes \mathbb{1}_{l_{6o}} \otimes |0\rangle\langle 0|_{m3} \otimes |0\rangle\langle 0|_{m4} \otimes (\mathbb{1} - |0\rangle\langle 0|_{m5}), \tag{18}$$

$$\hat{\Pi}_4^{(\mathrm{out})} = \mathbb{1}_{l_{1o}} \otimes \ldots \otimes \mathbb{1}_{l_{6o}} \otimes (\mathbb{1} - |0\rangle\langle 0|_{m3}) \otimes (\mathbb{1} - |0\rangle\langle 0|_{m4}) \otimes |0\rangle\langle 0|_{m5}, \tag{19}$$

$$\hat{\Pi}_5^{(\mathrm{out})} = \mathbb{1}_{l_{1o}} \otimes \ldots \otimes \mathbb{1}_{l_{6o}} \otimes [(\mathbb{1} - |0\rangle\langle 0|_{m3}) \otimes |0\rangle\langle 0|_{m4} + |0\rangle\langle 0|_{m3} \otimes (\mathbb{1} - |0\rangle\langle 0|_{m4})] \otimes (\mathbb{1} - |0\rangle\langle 0|_{m5}). \tag{20}$$

By expanding the photon-number modes as $|n\rangle\langle n| = 1/n! a^{\dagger n}|0\rangle\langle 0|a^n$, these ideal POVM elements can then be propagated backwards through the lossy circuit to determine the complete POVM elements for the overall measurement apparatus, which we represent by $\hat{\Pi}_{\alpha\gamma}^{(\mathrm{in})}$. These back-propagated projectors, however, can be dramatically simplified using *a priori* knowledge of the system, that is, that the input loss modes l_{1i} to l_{6i} contain only the vacuum, and that the state ρ contains, for example, no more than two photons. The back-propagated projectors can therefore be *conditioned* using this information, which can be summarized by the following projector:

$$\hat{P} = (|0\rangle\langle 0| + |1\rangle\langle 1| + |2\rangle\langle 2|)_{m1} \otimes (|0\rangle\langle 0| + |1\rangle\langle 1| + |2\rangle\langle 2|)_{m2} \otimes |0\rangle\langle 0|_{l1i} \otimes \ldots \otimes |0\rangle\langle 0|_{l6i}. \tag{21}$$

This allows us to calculate the final measurement POVM elements according to

$$\hat{\Pi}_{\alpha\gamma} = \hat{P}\hat{\Pi}_{\alpha\gamma}^{(\mathrm{in})}\hat{P}. \tag{22}$$

We note that when the transmissivities η_1 to η_4 are pair-wise symmetric so that $\eta_1 = \eta_2$ and $\eta_3 = \eta_4$, the situation is further simplified, because the total population in the loss modes is not a function of the phases θ and ϕ, since every possible path to the detectors experiences the same loss regardless of the phase settings. This approximation corresponds to the standard bulk-optics scenario where loss does not typically depend on the occupied mode, for example, in a free-space polarization-based interferometer where loss is not normally polarization dependent.

6. Conclusion

Integrated photonics is one of several extremely promising technologies whose aims are to allow the exploration of the fundamental properties of quantum mechanics and the application of these phenomena to real tasks. Although much progress has been made in investigating the individual modules necessary to perform integrated experiments, there has been little work on managing the interfaces between them in order to achieve full integration. In particular, the effects of loss in quantum devices, which differ significantly from the effects of loss in classical devices, have been largely overlooked to date, although they are now the single largest hurdle confronting the field. In this paper we have explored a modular approach to integration and enumerated the requirements on each of state generation, manipulation and detection in the context of quantum-enhanced metrology. We have argued that the control of modes is key, both in order to optimize each individual module and to optimize the interfaces.

We have discussed sources based on SFWM and the necessary considerations that enable pure, single photons to be generated with high heralding efficiencies in a transverse spatial mode that is well matched to existing photonic circuit technology. We have shown how managing the spectral mode of the generated photons is critical to maximizing the heralding efficiency, demonstrating the tradeoff between this and state purity for a typically correlated source. We have also discussed how to construct programmable devices that are robust to fabrication imperfections and demonstrated a method that allows the characterization of individual beam splitters, even when they are embedded within a complex circuit. Finally, we have enumerated some of the possibilities for integrated detectors and introduced a framework that describes how to perform state tomography of a heralded state, allowing reconstruction of all photon number sub-spaces rather than post-selecting on a particular photon number sub-space. This framework ultimately allows the utility of a state for quantum-enhanced metrology to be assessed through the QCRB.

Acknowledgments

We acknowledge K Banaszek, C Silberhorn, U Dorner and R Demkowicz-Dobrzanski for fruitful discussions that have informed the progress of this work. This work was supported by the European Commission under the Integrated Project Quantum Interfaces, Sensors, and Communication based on Entanglement (Q-ESSENCE), the US European Office of Aerospace Research (FA8655-09-1-3020), the Engineering and Physical Sciences Research Council (EPSRC) (grant no. EP/H03031X/1), the Royal Society and by FONCICYT project no. 94142.

References

[1] Smith B J, Kundys D, Thomas-Peter N, Smith P G R and Walmsley I A 2009 Phase-controlled integrated photonic quantum circuits *Opt. Express* **17** 13516

[2] Matthews J C F, Politi A, Stefanov A and O'Brien J L 2009 Manipulation of multiphoton entanglement in waveguide quantum circuits *Nat. Photonics* **3** 346

[3] Peruzzo A *et al* 2010 Quantum walks of correlated photons *Science* **329** 1500–3

[4] Schreiber A, Cassemiro K N, Potoček V, Gábris A, Mosley P J, Andersson E, Jex I and Silberhorn C 2010 Photons walking the line: a quantum random walk with adjustable coin operations *Phys. Rev. Lett.* **104** 050502

[5] Politi A, Cryan M J, Rarity J G, Yu S and O'Brien J L 2008 Silica-on-silicon waveguide quantum circuits *Science* **320** 646
[6] Politi A, Matthews J C F and O'Brien J L 2009 Shor's quantum factoring algorithm on a photonic chip *Science* **325** 1221
[7] Anderson M E, McAlister D F, Raymer M G and Gupta M C 1997 Pulsed squeezed-light generation in $\chi^{(2)}$ nonlinear waveguides *J. Opt. Soc. Am.* B **14** 3180
[8] Banaszek K, U'Ren A B and Walmsley I A 2001 Generation of correlated photons in controlled spatial modes by downconversion in nonlinear waveguides *Opt. Lett.* **26** 1367
[9] U'Ren A B, Silberhorn C, Banaszek K and Walmsley I A 2004 Efficient conditional preparation of high-fidelity single photon states for fiber-optic quantum networks *Phys. Rev. Lett.* **93** 093601
[10] Chen J, Xiaoying L and Kumar P 2005 Two-photon-state generation via four-wave mixing in optical fibers *Phys. Rev.* A **72** 033801
[11] Xiaoying L, Voss P L, Sharping J E and Kumar P 2005 Optical-fiber source of polarization-entangled photons in the 1550 nm telecom band *Phys. Rev. Lett.* **94** 053601
[12] Sharping J E, Lee K F, Foster M A, Turner A C, Schmidt B S, Lipson M, Gaeta A L and Kumar P 2006 Generation of correlated photons in nanoscale silicon waveguides *Opt. Express* **14** 12388
[13] Garay-Palmett K, McGuinness H J, Cohen O, Lundeen J S, Rangel-Rojo R, U'Ren A B, Raymer M G, McKinstrie C J, Radic S and Walmsley I A 2007 Photon pair-state preparation with tailored spectral properties by spontaneous four-wave mixing in photonic-crystal fiber *Opt. Express* **15** 14870
[14] Avenhaus M, Eckstein A, Mosley P J and Silberhorn C 2009 Fiber-assisted single-photon spectrograph *Opt. Lett.* **34** 2873
[15] Chen J, Pearlman A J, Ling A, Fan J and Migdall A 2009 A versatile waveguide source of photon pairs for chip-scale quantum information processing *Opt. Express* **17** 6727
[16] Clemmen S, Huy K P, Bogaerts W, Baets R G, Emplit P and Massar S 2009 Continuous wave photon pair generation in silicon-on-insulator waveguides and ring resonators *Opt. Express* **17** 16558
[17] Mosley P J, Christ A, Eckstein A and Silberhorn C 2009 Direct measurement of the spatial-spectral structure of waveguided parametric down-conversion *Phys. Rev. Lett.* **103** 233901
[18] Smith B J, Mahou P, Cohen O, Lundeen J S and Walmsley I A 2009 Photon pair generation in birefringent optical fibers *Opt. Express* **17** 23589
[19] Levine Z H, Fan J, Chen J, Ling A and Migdall A 2010 Heralded, pure-state single-photon source based on a potassium titanyl phosphate waveguide *Opt. Express* **18** 3708
[20] Branczyk A M, Ralph T C, Helwig W and Silberhorn C 2010 Optimized generation of heralded Fock states using parametric down-conversion *New J. Phys.* **12** 063001
[21] Eckstein A, Christ A, Mosley P J and Silberhorn C 2011 Highly efficient single-pass source of pulsed single-mode twin beams of light *Phys. Rev. Lett.* **106** 013603
[22] Honjo T, Inoue K and Takahashi H 2004 Differential-phase-shift quantum key distribution experiment with a planar light-wave circuit Mach–Zehnder interferometer *Opt. Lett.* **29** 2797
[23] Takesue H and Inoue K 2005 Generation of 1.5 μm band time-bin entanglement using spontaneous fiber four-wave mixing and planar light–wave circuit interferometers *Phys. Rev.* A **72** 041804
[24] Marshall G D, Politi A, Matthews J C F, Dekker P, Ams M, Withford M J and O'Brien J L 2009 Laser written waveguide photonic quantum circuits *Opt. Express* **17** 12546–54
[25] Sansoni L, Sciarrino F, Vallone G, Mataloni P, Crespi A, Ramponi R and Osellame R 2010 Polarization entangled state measurement on a chip *Phys. Rev. Lett.* **20** 200503
[26] Peruzzo A, Laing A, Politi A, Rudolph T and O'Brien J L 2010 Multimode quantum interference of photons in multiport integrated devices arXiv:1007.1372
[27] Wu B, Hulbert J F, Lunt E J, Hurd K, Hawkins A R and Schmidt H 2010 Slow light on a chip via atomic quantum state control *Nat. Photonics* **4** 776
[28] Banaszek K and Walmsley I A 2003 Photon counting with a loop detector *Opt. Lett.* **28** 52
[29] Achilles D, Silberhorn C and Walmsley I A 2006 Direct, loss-tolerant characterization of nonclassical photon statistics *Phys. Rev. Lett.* **97** 043602

[30] Natarajan C M, Peruzzo A, Miki S, Sasaki M, Wang Z, Baek B, Nam S, Hadfield R H and O'Brien J L 2010 Operating quantum waveguide circuits with superconducting single-photon detectors *Appl. Phys. Lett.* **96** 211101
[31] Varnava M, Browne D E and Rudolph T 2006 Loss tolerance in one-way quantum computation via counterfactual error correction *Phys. Rev. Lett.* **97** 120501
[32] Varnava M, Browne D E and Rudolph T 2008 How good must single photon sources and detectors be for efficient linear optical quantum computation? *Phys. Rev. Lett.* **100** 060502
[33] Thomas-Peter N L, Smith B J, Dorner U and Walmsley I A 2010 Real-world quantum sensors: evaluating resources for precision measurement arXiv:1007.0870
[34] Datta A, Zhang L, Smith B J and Walmsley I A 2010 Quantum metrology with imperfect states and detectors arXiv:1012.0539
[35] Pittman T B, Fitch M J, Jacobs B C and Franson J D 2003 Experimental controlled-NOT logic gate for single photons in the coincidence basis *Phys. Rev.* A **68** 032316
[36] Laing A, Peruzzo A, Politi A, Verde M R, Halder M, Ralph T C, Thompson M G and O'Brien J L 2010 High-fidelity operation of quantum photonic circuits *Appl. Phys. Lett.* **97** 211109
[37] Lanyon B P, Weinhold T J, Langford N K, Barbieri M, James D F V, Gilchrist A and White A G 2007 Experimental demonstration of a compiled version of Shor's algorithm with quantum entanglement *Phys. Rev. Lett.* **99** 250505
[38] Walther P, Resch K J, Rudolph T, Schenck E, Weinfurter H, Vedral V, Aspelmeyer M and Zeilinger A 2005 Experimental one-way quantum computing *Nature* **434** 169
[39] Zhang Q, Goebel A, Wagenknecht C, Chen Y A, Zhao B, Yang T, Mair A, Schmiedmayer J and Pan J W 2006 Experimental quantum teleportation of a two-qubit composite system *Nat. Phys.* **2** 678
[40] Prevedel R, Walther P, Tiefenbacher F, Böhi P, Kaltenbaek R, Jennewein T and Zeilinger A 2007 High-speed linear optics quantum computing using active feed-forward *Nature* **445** 65
[41] Gao W B, Xu P, Yao X C, Gühne O, Cabello A, Lu C Y, Peng C Z, Chen Z B and Pan J W 2010 Experimental realization of a controlled-NOT gate with four-photon six-qubit cluster states *Phys. Rev. Lett.* **104** 020501
[42] Raymer M G, Noh J, Banaszek K and Walmsley I A 2005 Pure-state single-photon wave-packet generation by parametric down-conversion in a distributed microcavity *Phys. Rev.* A **72** 023825
[43] Christ A, Eckstein A, Mosley P J and Silberhorn C 2009 Pure single photon generation by type-i PDC with backward-wave amplification *Opt. Express* **17** 3441
[44] Watanabe K, Hashizume Y, Nasu Y, Kohtoku M, Itoh M and Inoue Y 2008 Ultralow power consumption silica-based PLC-VOA/switches *J. Lightw. Technol.* **26** 2235
[45] Schmidt H, Dongliang Y, Barber J P and Hawkins A R 2005 Hollow-core waveguides and 2-d waveguide arrays for integrated optics of gases and liquids *Sel. Top. Quantum Electron.* **11** 519–27
[46] Braunstein S L and Caves C M 1994 Statistical distance and the geometry of quantum states *Phys. Rev. Lett.* **72** 3439–43
[47] Dorner U, Demkowicz-Dobrzanski R, Smith B J, Lundeen J S, Wasilewski W, Banaszek K and Walmsley I A 2009 Optimal quantum phase estimation *Phys. Rev. Lett.* **102** 040403
[48] Mitchell M W, Lundeen J S and Steinberg A M 2004 Super-resolving phase measurements with a multiphoton entangled state *Nature* **429** 161–4
[49] Eisenberg H S, Hodelin J F, Khoury G and Bouwmeester D 2005 Multiphoton path entanglement by nonlocal bunching *Phys. Rev. Lett.* **94** 090502
[50] Higgins B L, Berry D W, Bartlett S D, Wiseman H M and Pryde G J 2007 Entanglement-free Heisenberg-limited phase estimation *Nature* **450** 393–6
[51] Kim H, Park H S and Choi S-K 2009 Three-photon N00N states generated by photon subtraction from double photon pairs *Opt. Express* **17** 19720–6
[52] Afek I, Ambar O and Silberberg Y 2010 High-noon states by mixing quantum and classical light *Science* **328** 879–81
[53] Walther P, Aspelmeyer M and Zeilinger A 2007 Heralded generation of multiphoton entanglement *Phys. Rev.* A **75** 012313

[54] McCusker K T and Kwiat P G 2009 Efficient optical quantum state engineering *Phys. Rev. Lett.* **103** 163602
[55] Kacprowicz M, Demkowicz-Dobrzanski R, Wasilewski W, Banaszek K and Walmsley I A 2010 Experimental quantum-enhanced estimation of a lossy phase shift *Nat. Photonics* **4** 357–60
[56] Holland M J and Burnett K 1993 Interferometric detection of optical phase shifts at the Heisenberg limit *Phys. Rev. Lett.* **71** 1355–8
[57] Nunn J, Walmsley I A, Raymer M G, Surmacz K, Waldermann F C, Wang Z and Jaksch D 2007 Mapping broadband single-photon wave packets into an atomic memory *Phys. Rev.* A **75** 011401
[58] Reim K F, Nunn J, Lorenz V O, Sussman B J, Lee K C, Langford N K, Jaksch D and Walmsley I A 2010 Towards high-speed optical quantum memories *Nat. Photonics* **4** 218
[59] Reim K F, Michelberger P, Lee K C, Nunn J, Langford N K and Walmsley I A 2010 Single-photon-level quantum memory at room temperature arXiv:1010.3975
[60] Ralph T C, Langford N K, Bell T B and White A G 2002 Linear optical controlled-NOT gate in the coincidence basis *Phys. Rev.* A **65** 062324
[61] Barbieri M, Weinhold T J, Lanyon B P, Gilchrist A, Resch K J, Almeida M P and White A G 2009 Parametric downconversion and optical quantum gates: two's company, four's a crowd *J. Mod. Opt.* **56** 209
[62] Avenhaus M, Coldenstrodt-Ronge H B, Laiho K, Mauerer W, Walmsley I A and Silberhorn C 2008 Photon number statistics of multimode parametric down-conversion *Phys. Rev. Lett.* **101** 053601
[63] Grice W P, U'Ren A B and Walmsley I A 2001 Eliminating frequency and space-time correlations in multiphoton states *Phys. Rev.* A **64** 063815
[64] U'Ren A B, Banaszek K and Walmsley I A 2003 Photon engineering for quantum information processing *Quantum Inf. Comput.* **3** 480
[65] U'Ren A B, Silberhorn C, Banaszek K, Walmsley I A, Erdmann R, Grice W P and Raymer M G 2005 Generation of pure-state single-photon wavepackets by conditional preparation based on spontaneous parametric downconversion *Laser Phys.* **15** 146
[66] Mosley P J, Lundeen J S, Smith B J, Wasylczyk P, U'Ren A B, Silberhorn C and Walmsley I A 2008 Heralded generation of ultrafast single photons in pure quantum states *Phys. Rev. Lett.* **100** 133601
[67] Cohen O, Lundeen J S, Smith B J, Puentes G, Mosley P J and Walmsley I A 2009 Tailored photon-pair generation in optical fibers *Phys. Rev. Lett.* **102** 123603
[68] Halder M, Fulconis J, Cemlyn B, Clark A, Xiong C, Wadsworth W J and Rarity J G 2009 Nonclassical 2-photon interference with separate intrinsically narrowband fibre sources *Opt. Express* **17** 4670
[69] Söller C, Brecht B, Mosley P J, Zang L Y, Podlipensky A, Joly N Y, Russell P St J and Silberhorn C 2010 Bridging visible and telecom wavelengths with a single-mode broadband photon pair source *Phys. Rev.* A **81** 031801
[70] Herrmann H, Büchter K-D, Ricken R and Sohler W 2010 Tunable integrated electro-optic wavelength filter with programmable spectral response *J. Lightw. Technol.* **28** 1051
[71] Sanders B C, Milburn G J and Zhang Z 1997 Optimal quantum measurements for phase-shift estimation in optical interferometry *J. Mod. Opt.* **44** 1309
[72] Lita A E, Calkins B, Pellouchoud L A, Miller A J and Nam S W 2010 Superconducting transition-edge sensors optimized for high-efficiency photon-number resolving detectors *Proc. SPIE* **7681** 76810D
[73] Lundeen J S, Feito A, Coldenstrodt-Ronge H, Pregnell K L, Silberhorn C, Ralph T C, Eisert J, Plenio M B and Walmsley I A 2009 Tomography of quantum detectors *Nat. Phys.* **5** 27
[74] Feito A, Lundeen J S, Coldenstrodt-Ronge H, Eisert J, Plenio M B and Walmsley I A 2009 Measuring measurement: theory and practice *New J. Phys.* **11** 093038
[75] Worsley A P, Coldenstrodt-Ronge H, Lundeen J S, Mosley P J, Smith B J, Puentes G, Thomas-Peter N and Walmsley I A 2009 Absolute efficiency estimation of photon-number-resolving detectors using twin beams *Opt. Express* **17** 4397
[76] Smithey D T, Beck M, Raymer M G and Faridani A 1993 Measurement of the wigner distribution and the density matrix of a light mode using optical homodyne tomography: application to squeezed states and the vacuum *Phys. Rev. Lett.* **70** 1244

[77] James D F V, Kwiat P G, Munro W J and White A G 2001 Measurement of qubits *Phys. Rev.* A **64** 052312
[78] Hradil Z, Mogilevtsev D and Rehacek J 2006 Biased tomography schemes: an objective approach *Phys. Rev. Lett.* **96** 230401
[79] de Burgh M D, Langford N K, Doherty A C and Gilchrist A 2008 Choice of measurement sets in qubit tomography *Phys. Rev.* A **78** 052122
[80] Adamson R B A and Steinberg A M 2010 Improving quantum state estimation with mutually unbiased bases *Phys. Rev. Lett.* **105** 030406
[81] Ling A, Soh K P, Lamas-Linares A and Kurtsiefer C 2006 Experimental polarization state tomography using optimal polarimeters *Phys. Rev.* A **74** 022309
[82] Nunn J, Smith B J, Puentes G and Walmsley I A 2010 Optimal experiment design for quantum state tomography: fair, precise, and minimal tomography *Phys. Rev.* A **81** 042109
[83] Boyd S and Vandenberghe L 2004 *Convex Optimization* (Cambridge: Cambridge University Press)
[84] Achilles D, Silberhorn C, Sliwa C, Banaszek K, Walmsley I A, Fitch M J, Jacobs B C, Pittman T B and Franson J D 2004 Photon-number-resolving detection using time-multiplexing *J. Mod. Opt.* **51** 1499